AChBP-targeted α-conotoxin correlates distinct binding orientations with nAChR subtype selectivity

Sébastien Dutertre, Chris Ulens, Regina Büttner, Alexander Fish, René van Elk, Yvonne Kendel, Gene Hopping, Paul F Alewood, Christina Schroeder, Annette Nicke, et al.

The EMBO Journal (2007) 26, 3858–3867 | © 2007 European Molecular Biology Organization | Some Rights Reserved 0261-4189/07
www.embojournal.org

THE EMBO JOURNAL

EMBO open

AChBP-targeted α-conotoxin correlates distinct binding orientations with nAChR subtype selectivity

Sébastien Dutertre[1,6,7], Chris Ulens[2,6], Regina Büttner[3], Alexander Fish[2], René van Elk[4], Yvonne Kendel[5], Gene Hopping[1], Paul F Alewood[1], Christina Schroeder[1], Annette Nicke[3], August B Smit[4], Titia K Sixma[2,*] and Richard J Lewis[1,*]

[1]Institute for Molecular Bioscience, The University of Queensland, Brisbane, Queensland, Australia, [2]Division of Molecular Carcinogenesis and Center for Biomedical Genetics, Netherlands Cancer Institute, Plesmanlaan, CX Amsterdam, The Netherlands, [3]Department of Neurochemistry, Max Planck Institute for Brain Research, Deutschordenstrasse 46, Frankfurt am Main, Germany, [4]Department of Molecular and Cellular Neurobiology, Center for Neurogenomics and Cognitive Research, Vrije Universiteit, Amsterdam, The Netherlands and [5]Zentrum der Rechtsmedizin, University of Frankfurt, Frankfurt am Main, Germany

Neuronal nAChRs are a diverse family of pentameric ion channels with wide distribution throughout cells of the nervous and immune systems. However, the role of specific subtypes in normal and pathological states remains poorly understood due to the lack of selective probes. Here, we used a binding assay based on acetylcholine-binding protein (AChBP), a homolog of the nicotinic acetylcholine ligand-binding domain, to discover a novel α-conotoxin (α-TxIA) in the venom of *Conus textile*. α-TxIA bound with high affinity to AChBPs from different species and selectively targeted the $\alpha_3\beta_2$ nAChR subtype. A co-crystal structure of Ac-AChBP with the enhanced potency analog TxIA(A10L), revealed a 20° backbone tilt compared to other AChBP–conotoxin complexes. This reorientation was coordinated by a key salt bridge formed between Arg5 (TxIA) and Asp195 (Ac-AChBP). Mutagenesis studies, biochemical assays and electrophysiological recordings directly correlated the interactions observed in the co-crystal structure to binding affinity at AChBP and different nAChR subtypes. Together, these results establish a new pharmacophore for the design of novel subtype-selective ligands with therapeutic potential in nAChR-related diseases.

*Corresponding authors. RJ Lewis, Institute for Molecular Bioscience, The University of Queensland, Carmodty Rd, Brisbane, Queensland 4072, Australia. Tel.: +617 3346 2984; Fax: +617 3346 2101; E-mail: r.lewis@imb.uq.edu.au or TK Sixma, Division of Molecular Carcinogenesis and Center for Biomedical Genetics, Netherlands Cancer Institute, Plesmanlaan, 1066 CX Amsterdam, The Netherlands. E-mail: t.sixma@nki.nl
[6]These authors contributed equally to this work
[7]Present address: Max Planck Institute for Brain Research, Deutschordenstrasse 46, 60528 Frankfurt am Main, Germany.

Received: 6 February 2007; accepted: 12 June 2007; published online: 26 July 2007

The EMBO Journal (2007) **26,** 3858–3867. doi:10.1038/sj.emboj.7601785; Published online 26 July 2007
Subject Categories: structural biology
Keywords: acetylcholine binding protein; conotoxin; cys-loop receptor; ion channel; nicotinic acetylcholine receptors

Introduction

Acetylcholine binding proteins (AChBPs) have been identified from different snails, including *Lymnaea stagnalis* (Smit *et al*, 2001), *Aplysia californica* (Hansen *et al*, 2004; Celie *et al*, 2005a) and *Bulinus truncatus* (Celie *et al*, 2005b). AChBPs are homologous to the ligand-binding domains (LBDs) of the nicotinic acetylcholine receptors (nAChRs) and pharmacological characterization has demonstrated that their properties most closely resemble those of the α_7 nAChRs (Smit *et al*, 2001), which also function as homopentamers. Crystallization and structure determination of AChBPs (Hansen *et al*, 2005; Celie *et al*, 2005a, b) from these different species has revealed a highly conserved architecture, despite the relatively low sequence identity between different AChBPs. A similar level of sequence homology is found with the LBDs of members of the ligand-gated ion channel family, comprising the nAChRs, GABA-A/C receptors, 5-HT3 and glycine receptors. AChBP has been co-crystallized with prototype ligands that are known to bind to nAChRs, thus establishing the structural determinants for ligand recognition of agonists such as nicotine and carbamylcholine (Celie *et al*, 2004), and antagonists such as different α-conotoxins (Celie *et al*, 2005a; Ulens *et al*, 2006) and long-chain snake neurotoxins (Bourne *et al*, 2005), and partial agonists such as lobeline (Hansen *et al*, 2005). Comparison of these different crystal structures has revealed conformational changes occurring upon ligand binding, and has allowed predictions as to how these conformational changes may be coupled to channel opening through the loops that form the interface with the transmembrane domain in the nAChR.

The venoms from cone snails are a rich source of peptides with high affinity for several voltage- and ligand-gated ion channels, including nAChRs (Olivera *et al*, 1990). Recently, we and others have solved crystal structures of Ac-AChBP in complex with two different α-conotoxins, namely PnIA(A10L D14K) (Celie *et al*, 2005a) and ImI (Hansen *et al*, 2005; Ulens *et al*, 2006). These two conotoxins greatly differ in their selectivity among AChBPs and comparison of the toxin–receptor interface in both complexes provided structural insight into the molecular determinants of ligand selectivity (Ulens *et al*, 2006).

In addition to being remarkable probes for structural studies, α-conotoxins also have therapeutic potential (Lewis and Garcia, 2003). For example, Vc1.1, the first α-conotoxin being developed to treat neuropathic pain also caused an accelerated recovery of injured neurons (Satkunanathan *et al*, 2005). Recently, Vc1.1 was shown to specifically target α_9/α_{10} nAChRs, providing a rationale for its analgesic property (Vincler *et al*, 2006). Determining the specific roles of the multiple nAChR subtypes under physiological or pathological conditions and the development of drugs to treat nAChR-related disorders, such as Parkinson's disease and nicotine addiction, requires further subtype-selective ligands.

In this study, we used Ls-AChBP as a bait to discover the novel α-conotoxin TxIA from *Conus textile*. Pharmacological characterization shows that TxIA binds with very high affinity to AChBPs from different species, as well as selectively to certain subtypes of neuronal nAChRs. The co-crystal structure of Ac-AChBP with a more potent analog TxIA(A10L), revealed that this α-conotoxin adopts a different binding orientation to that observed for other α-conotoxin–AChBP complexes. A salt bridge between Arg5 in TxIA(A10L) and Asp195 of Ac-AChBP was visible in the structure and the importance of this interaction for AChBP binding and nAChR selectivity was established using binding assays, surface plasmon resonance (SPR) and electrophysiological experiments with mutant receptors and conotoxin analogs. These results highlight the potential of an AChBP screen to discover novel ligands acting at the nAChR and provide a new pharmacophore for the design of ligands with improved subtype selectivity.

Results

Identification and pharmacological characterization of α-conotoxin TxIA

We tested the activity of crude venoms obtained from more than 30 species of Australian cone snails against Ls-AChBP in a competitive binding assay with radiolabeled α-bungarotoxin (^{125}I-Bgt). We chose the venom of cone snails as our 'combinatorial library of ligands', as all species tested so far were shown to contain at least one nAChR ligand among the 50–200 unique conopeptides known to occur in each venom (McIntosh *et al*, 1999). Accordingly, the venoms from all species showed some competition in our Ls-AChBP-binding assay (Figure 1A). We focused on *C. textile* venom, as full competition with ^{125}I-Bgt was observed, indicating the presence of a high affinity or abundant ligand (Figure 1A). Upon isolation the active compound was found to be in low abundance, indicating that it was relatively potent (Figure 1B). Mass spectrometry revealed a monoisotopic mass of 1656.68 Da, similar in size to previously isolated α-conotoxins. N-terminal sequencing revealed a novel 16 amino-acid peptide belonging to the 4/7 α-conotoxin family, which we named α-conotoxin TxIA (Table I). The calculated mass (1661.67 Da) was consistent with two disulfide bonds (–4 Da) and an amidated C terminus (–1 Da), two post-translational modifications common in this class of conotoxins (Loughnan and Alewood, 2004).

Synthetic analogs of TxIA were assembled using Boc chemistry for further analysis and to determine the cysteine connectivity. The 'native' conformation (connectivity 1–3,

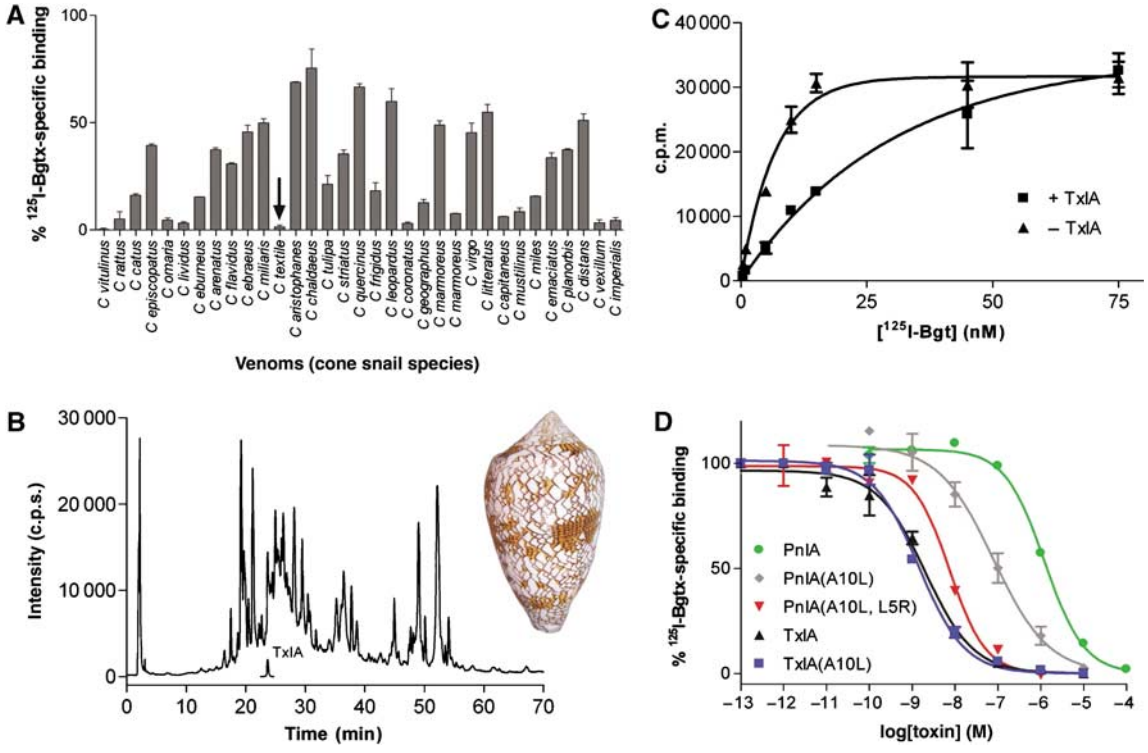

Figure 1 Isolation and characterization of α-conotoxin TxIA. (**A**) Ls-AChBP screening for α-conotoxins in venoms of 30 species of Australian cone snails. (**B**) LC-MS profile of the crude venom of *C. textile*. TxIA was isolated as a minor component shown in the extracted ions for this peptide. Inset shows a shell of *C. textile*. (**C**) Saturation binding experiments revealed a competitive interaction of TxIA with Ls-AChBP. When an $\sim IC_{50}$ concentration of TxIA was added, the K_d of ^{125}I-Bgt shifted from 3.5 to 40 nM, whereas the B_{max} remained unaffected. (**D**) Displacement of ^{125}I-Bgt from Ls-AChBP by α-conotoxins TxIA, PnIA and analogs (plot with all fixed to 100% in curve fit). Data in (A), (C) and (D) represent the mean ± s.e.m. of duplicate data obtained in three separate experiments.

Table I Binding affinities (nM) of α-conotoxins for Ls-AChBP

α-Conotoxin	Sequence	Target	K_i (CI)	Hill slope
TxIA	**GCC**SR**P**P**C**IANNPDL**C**	AChBP > $\alpha_3\beta_2 > \alpha_7$	1.7 (1.1–2.8)	−0.79
PnIA(A10L)	G**CC**SLPP**C**ALNNPDY**C**	$\alpha_7 > \alpha_3\beta_2$	80 (44–148)	−1.04
EI	RDO**GCC**YH**P**T**C**NMSNPQI**C**	muscle	496 (430–572)	−0.70
PnIA	**GCC**SL**P**P**C**AANNPDY**C**	$\alpha_3\beta_2 > \alpha_7$	1000 (768–1303)	−0.93
MII	**GCC**SN**P**V**C**HLEHSNL**C**	$\alpha_3\alpha_6\beta_2$	1093 (861–1388)	−0.84
[Y15]-EpI	**GCC**SD**P**R**C**NMNNPDY**C**	$\alpha_3\beta_2/\beta_4$	6976 (5704–8532)	−0.87

Bold indicate conserved residues.

2–4) and the 'ribbon' fold (connectivity 1–4, 2–3) were both able to displace ^{125}I-Bgt bound to Ls-AChBP. However, whereas the native fold displayed a K_i of 1.7 nM, the ribbon fold was 380-fold less potent (Supplementary Figure 1). Therefore, the connectivity is assumed to be 1–3, 2–4 in the venom-isolated α-TxIA, as was found in all other α-conotoxins identified to date. Comparison with other synthetic α-conotoxins known to bind nAChRs revealed that α-TxIA is 50-fold more potent than the α_7 nAChR-selective PnIA(A10L) in displacing ^{125}I-Bgt at Ls-AChBP (Table I). The muscle nAChR-selective EI displayed an intermediate K_i value of 496 nM, followed in decreasing order of potency by the $\alpha_3\beta_2$ nAChR-selective PnIA (1.0 μM) and the $\alpha_6/\alpha_3\beta_2$ nAChR-selective MII (1.1 μM), whereas EpI had the lowest affinity (7 μM). Previously, pH was shown to influence the potency of the histidine-containing α-MII in functional assays (Everhart *et al*, 2004). This effect also applies to MII binding to Ls-AChBP (Spearman's test, $P<0.01$), whereas the other toxins were most active at physiological pH (Supplementary Figure 2). In a saturation-binding experiment, addition of an $\sim IC_{50}$ concentration of native α-TxIA increased the K_d of ^{125}I-Bgt from 3.5 to 40 nM without affecting the maximum binding B_{max}, indicative of a competitive binding interaction (Figure 1C). α-TxIA was also tested on rat brain membranes using ^{125}I-Bgt and ^{3}H-epibatidine as tracers to determine the affinity for α_7 and mostly $\alpha_4\beta_2$ neuronal nAChRs, respectively. α-TxIA displaced ^{125}I-Bgt with a K_i of 1.2 μM (α_7 nAChR), but failed to displace ^{3}H-epibatidine using up to 10 μM of peptide. Finally, α-TxIA was tested in a functional assay on heterologously expressed mammalian nAChRs (Figure 2). α-TxIA potently inhibited nicotine-induced current at the $\alpha_3\beta_2$ nAChR ($IC_{50} = 3.5$ nM) and α_7 nAChRs ($IC_{50} = 392$ nM), but had no activity at the $\alpha_4\beta_2$ nAChR and muscle nAChR at concentrations up to 10 μM. Thus, α-TxIA is among the most $\alpha_3\beta_2$-selective toxins identified.

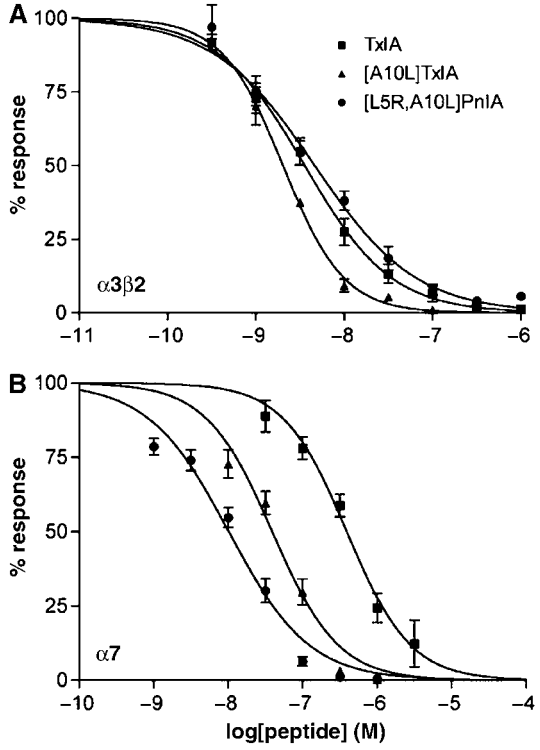

Figure 2 Antagonist activity of α-conotoxin TxIA and analogs at oocyte-expressed rat $\alpha_3\beta_2$ (**A**) and α_7 (**B**) nAChRs. Oocytes were clamped at −70 mV and 100 μM ACh ($\alpha_3\beta_2$) or nicotine (α_7) were applied for 2 s in 4 min intervals. Toxins were applied for 3 min. Data are represented as the mean ± s.e.m. of at least four oocytes.

Structure activity relationships

The sequence of α-TxIA was compared to previously identified 4/7 α-conotoxins (Table I). Interestingly, only three residues are different from α-conotoxin PnIA, yet PnIA is 600-fold less potent than TxIA at Ls-AChBP. To identify which of these residues conferred the high affinity at Ls-AChBP, we synthesized PnIA and TxIA mutants covering two of the three differences (Figure 1D and Table II). A third difference at position 15 was not investigated, as it was located outside the binding site identified in the co-crystal structure of Ac-AChBP with PnIA(A10L D14K) (Celie *et al*, 2005a). For the mutants tested, PnIA(A10L) had 12.5-fold higher affinity at Ls-AChBP, 20-fold higher affinity at the α_7 nAChR, but 10-fold reduced affinity at the $\alpha_3\beta_2$ nAChR (Hogg *et al*, 1999; Luo *et al*, 1999; Dutertre *et al*, 2005) (Table II). In contrast, TxIA(A10L) had similar potency to native TxIA at Ls-AChBP (Figure 1D and Table II), suggesting that Ile9 (Ala in PnIA) is able to substitute for Leu10 in PnIA(A10L) in the conserved hydrophobic patch that we have shown previously interacts with the complementary binding site of the nAChR (Dutertre *et al*, 2005). Despite the lack of effect on Ls-AChBP affinity, TxIA(A10L) was 12- and 2-fold more potent at the α_7 and $\alpha_3\beta_2$ nAChRs, respectively (Figure 2). Thus, a long-chain hydrophobic residue (Leu or Ile) at position 9 or 10 is important for high-affinity binding of TxIA and PnIA to Ls-AChBP and the α_7 nAChRs, but not $\alpha_3\beta_2$ nAChRs. A second difference is a Leu in position 5 of PnIA compared with an Arg in TxIA. As this position is well placed to directly interact with the receptor (Dutertre *et al*, 2005), this change in the physical property and length of the side chain could be an important contributor to high-affinity binding to Ls-AChBP. In support of this hypothesis, EI also has high affinity for Ls-AChBP and a positive charge in the equivalent position, whereas the low affinity [Y15]-EpI has a negatively charged

aspartic acid at this position. In agreement with these observations, PnIA(L5R A10L) had 220-fold increased affinity for Ls-AChBP compared to PnIA, clearly demonstrating the important role of Arg5 for high-affinity binding to Ls-AChBP (Figure 1D and Table II). The role of this residue appears also important for $\alpha_3\beta_2$ nAChR binding (10-fold increased affinity of PnIA(L5R A10L) compared to PnIA(A10L) at $\alpha_3\beta_2$ nAChR), but not for the α_7 nAChR (same affinity compared to PnIA(A10L)), suggesting that Arg5 interacts with Ls-AChBP and $\alpha_3\beta_2$ nAChRs in a similar manner (Figure 2 and Table II).

Crystal structure of Ac-AChBP in complex with TxIA(A10L)

To gain further insight into the nature of the interactions of α-TxIA with AChBP and their contribution to high affinity binding, we solved the crystal structure of Ac-AChBP in complex with the most potent TxIA analog, TxIA(A10L). Co-crystals were initially obtained with Ls-AChBP, Bt-AChBP and Ac-AChBP, but the latter gave diffraction data of better quality (see Supplementary Table I for statistics). TxIA(A10L) has comparable affinities to displace ^{3}H-epibatidine from *Lymnaea* and *Aplysia* AChBPs (data not shown). The structure of the complex was determined at 2.4 Å resolution (Figure 3A) and solved by molecular replacement. The asymmetric unit contains two pentamers and all binding sites were occupied by TxIA(A10L). The structure of Ac-AChBP in complex with TxIA(A10L) is very similar to other α-conotoxin complexes, with r.m.s.d. of 0.73 Å (1023 C_α atoms) upon superposition with the complex of Ac-AChBP with PnIA(A10L D14K) (Celie *et al*, 2005a) and 0.67 Å (1024 C_α atoms) for the Ac-AChBP complex with ImI (Ulens *et al*, 2006). The r.m.s.d. between monomers in the Ac-AChBP–TxIA(A10L) complex is 0.34 ± 0.04 Å. TxIA(A10L) binds with loop C displaced outward by a distance of 10.87 ± 0.50 Å as measured between the

Table II Potency (nM) of α-conotoxins TxIA, PnIA and analogues at AChBP and rat nAChRs

		^{125}I-Bgt binding	Electrophysiology	
α-Conotoxin	Sequence	Ls-AChBP, K_i (CI)	α_7 nAChR, IC_{50} (CI)	$\alpha_3\beta_2$ nAChR, IC_{50} (CI)
TxIA(A10L)	GCCS**R**PPC**I**LNNPD**L**C	1.1 (0.8–1.6)	39 (31–49)	2.0 (1.8–2.4)
TxIA	GCCS**R**PPC**I**ANNPD**L**C	1.7 (1.1–2.8)	392 (310–490)	3.6 (2.9–4.4)
PnIA(L5R-A10L)	GCCS**R**PPC**A**LNNPD**Y**C	6.2 (4.4–8.7)	10 (8.3–13)	4.6 (3.7–5.8)
PnIA(A10L)	GCCS**L**PPC**A**LNNPD**Y**C	80 (44–150)	13[a]	99[a]/55[b]
PnIA	GCCS**L**PPC**A**ANNPD**Y**C	1000 (770–1300)	252[a]	10[a]/8[b]

Residue bolded to indicate differences between PnIA and TxIA. Hill slope values were not significantly different from –1 (95% CI), except TxIA at AChBP (–0.93/–0.67), TxIA(A10L) at $\alpha_3\beta_2$ (–1.48/–1.04), and PnIA(L5R, A10L) at α_7 (–0.94/–0.67) and $\alpha_3\beta_2$ (–0.90/–0.62). Data from [a]Luo *et al* (1999) and [b]Dutertre *et al* (2005).

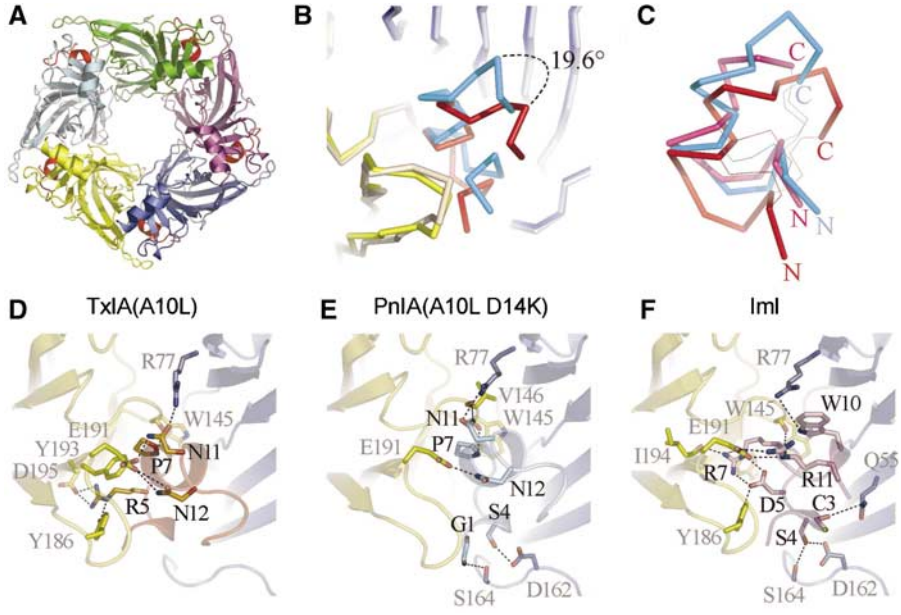

Figure 3 (**A**) Crystal structure of Ac-AChBP in complex with TxIA(A10L). The model is shown along the five-fold symmetry axis. α-Conotoxins are shown in red. (**B**) Superposition of the subunit interface from Ac-AChBP in complex with TxIA(A10L) and PnIA(A10L D14K). The principal face of the binding site is shown in shades of yellow, the complementary face in shades of blue. The superposition illustrates the different orientation of the conotoxin backbone in the binding pocket. PnIA(A10L D14K) is shown in blue, TxIA(A10L) in red. (**C**) Comparison of the different backbone orientations observed in co-crystal structures of Ac-AChBP with different α-conotoxins. TxIA(A10L), shown in red, is tilted by a 20° rotation around Pro7 with respect to PnIA(A10L D14K), shown in blue. The backbone orientation of α-conotoxin ImI, shown in magenta, is very similar to PnIA(A10L D14K) even though it is much shorter and forms a different network of interactions. Lines represent disulfide bridges. Detailed view of the molecular interactions that results in the different backbone orientations of (**D**) TxIA, (**E**) PhIA(A10L D14K) and (**F**) ImI within the binding site. The principal face of the binding site is shown in yellow, the complementary face in blue. The conotoxins are colored according to the color scheme in (C). Dashed lines represent hydrogen bonds or electrostatic interactions.

Cys188 C_α atom in the Ac-AChBP complex with TxIA(A10L) and the HEPES-bound Ac-AChBP structure (Celie *et al*, 2005a), similar to values measured for other α-conotoxin complexes. We previously observed ~3° rigid body rotations of the monomers in the Ac-AChBP complex with PnIA(A10L D14K) (Celie *et al*, 2005a), whereas these rotations were not seen in the Ac-AChBP complex with ImI (Ulens *et al*, 2006). The Ac-AChBP complex with TxIA(A10L) displays intermediate rotations (1–2°) of the monomers with respect to each other, which are most likely due to crystal contacts. The structure of TxIA(A10L) itself is very similar to other α-conotoxins and has an r.m.s.d. of 0.64±0.10 Å upon superposition with PnIA (PDB accession code 1PEN). TxIA(A10L) covers a surface area in the binding pocket of 788±18 Å^2, which is intermediate between the receptor–toxin interfaces formed with PnIA(A10L D14K) (827±32 Å^2) and ImI (679±15 Å^2) (Ulens *et al*, 2006).

We previously observed that PnIA(A10L D14K) and ImI share a similar orientation in the binding pocket, but differ dramatically in the nature of interactions formed within the binding site (Celie *et al*, 2005a; Ulens *et al*, 2006). Surprisingly, we see that TxIA(A10L) adopts an orientation that is different from those seen in other α-conotoxin–AChBP complexes. TxIA(A10L) is tilted 20° downward by a pivotal reorientation of the conotoxin around Pro7 (Figure 3B), which results in displacement by a distance of 4.72±0.83 Å, as measured between the C_α atoms at position 14 in the TxIA(A10L) and PnIA(A10L D14K) complexes. This different orientation of the conotoxin compared to those seen in other complexes (Figure 3C) is sustained by Arg5, which projects deep onto the principal face of the binding site and forms a hydrogen bond with Tyr186 and a salt bridge with Asp195 (Figure 3D), an interaction not seen in any of the other α-conotoxin complexes (Figure 3E and F). The structural data thus confirm a key role of Arg5 in the high-affinity binding of TxIA(A10L) to Ac-AChBP. The interface of TxIA(A10L) with the principal binding site is further characterized by the formation of four additional hydrogen bonds between TxIA and Pro7-Trp145 (loop B), TxIA and Asn12-Glu191 (loop C), and TxIA Pro7 and Asn11-Tyr193 (loop C) (Figure 3D). TxIA Pro7 also seems to play a dominant role in forming extensive van der Waals interactions with residues of the principal face that are not involved in contacts with PnIA(A10L D14K), namely Tyr91 (loop A), and Ser144, Trp145, Val146 and Tyr147 (loop B). In contrast, interaction of TxIA(A10L) with residues of the complementary face are similar to those seen in the Ac-AChBP complex with PnIA(A10L D14K) and are mostly hydrophobic in nature.

Comparison of the different AChBP–conotoxin complexes reinforces the notion that α-conotoxins can use different surface contacts to interact with the principal binding site (Figure 4A), whereas the surface area that contacts the complementary face of the binding site remains relatively conserved (Figure 4B). The calculated surface area of conotoxin ImI (1221±13 Å^2), for example, is smaller than PnIA(A10L D14K) (1508±17 Å^2) and TxIA(A10L) (1488±29 Å^2), but they all share a hydrophobic patch on one face of their surface that projects on the complementary binding site. On the other hand, ImI has two arginine residues (Arg7 and Arg11) that protrude into the principal binding site, a surface property not present in PnIA(A10L D14K). TxIA(A10L) seems to have surface properties that are intermediate between ImI and PnIA(A10L D14K), even though TxIA and PnIA are the same length and TxIA has the relatively exposed Arg5.

Functional importance of an electrostatic interaction for high affinity binding of α-conotoxins to AChBPs and $\alpha_3\beta_2$ nAChRs

Structure–activity relationships between TxIA analogs indicated an important role for Arg5 in the high-affinity binding of TxIA to AChBPs. Indeed, incorporation of an Arg residue in PnIA(A10L) at the equivalent position enhanced the affinity for Ls-AChBP that approached TxIA(A10L) affinity, with the tight electrostatic interaction between Arg5 of TxIA(A10L) and Asp195 of Ac-AChBP seen in our co-crystal structure

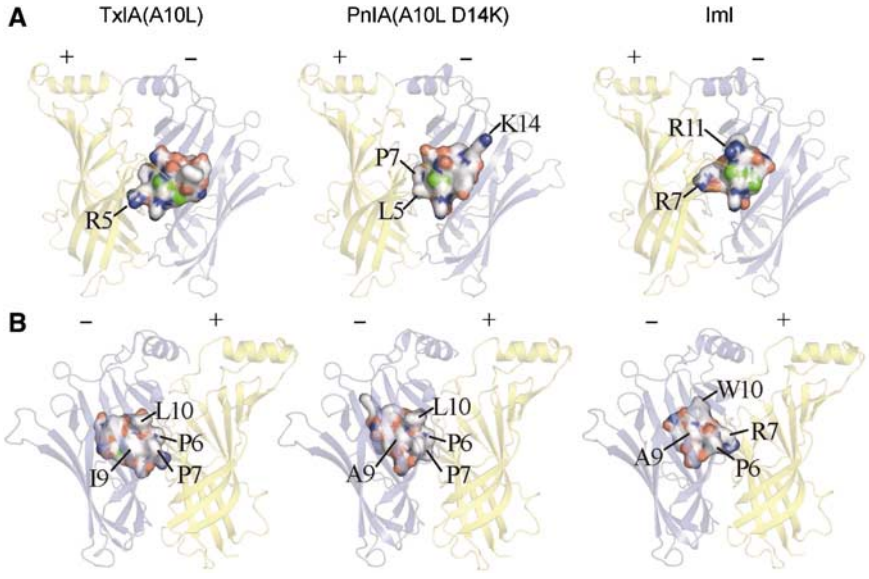

Figure 4 Surface representation of the three α-conotoxins that have been co-crystallized with Ac-AChBP. The surface of the α-conotoxin facing the principal binding site is shown in (**A**), the complementary binding site in (**B**). Ac-AChBP is shown in a transparent view for clarity. The principal subunit (+) of Ac-AChBP is shown in yellow, the complementary subunit (−) in blue.

explaining this effect. To further confirm this interaction, we mutated Asp195 in Ac-AChBP to Ala, Asn and Lys (unfortunately, insufficient Ac-AChBP D195K was expressed to allow a complete pharmacological characterization). In a competition assay, D195A and D195N showed binding properties for nicotine and acetylcholine that are comparable to wt Ac-AChBP (K_i nicotine $= 0.68 \pm 0.10\,\mu M$ and $0.81 \pm 0.13\,\mu M$ for D195A and D195N, respectively). However, TxIA and TxIA(A10L) showed a 30- to 50-fold reduction in affinity for the D195A and D195N mutants (Figure 5A). A similar reduction was also observed for PnIA(L5R A10L). In contrast, the affinity of PnIA(A10L D14K), which lacks an Arg at position 5, for D195A and D195N remained virtually unchanged. In addition, we compared the kinetic behavior of TxIA analogs on Ac-AChBP and the D195A mutant using SPR. In agreement with results from the binding assay, we observe an approximately sixfold acceleration in the dissociation rate for Arg5-containing α-conotoxins TxIA, TxIA(A10L) and PnIA(L5R A10L), whereas the dissociation kinetics for PnIA(A10L D14K) were unaffected by the D195A mutation (Figure 5B). These results provide strong evidence that the observed drop in affinity for Arg5-containing analogs at D195A can be directly attributed to the loss of an energetically favorable interaction with Asp195, which stabilizes Arg5-containing α-conotoxins in their bound position.

To extrapolate the functional importance of this electrostatic interaction to mammalian nAChRs, we introduced the equivalent D197A and D195A mutations in $\alpha_3\beta_2$ and α_7 nAChRs, respectively, and compared the potency of TxIA analogs by two-electrode voltage clamp analysis on the oocyte expressed mutant receptors (Figure 5C). In agreement with the results obtained with the Ac-AChBP mutants, we see that Arg5-containing conotoxins had 200- to 500-fold decreased activity at D197A-$\alpha_3\beta_2$. Together, these results show that the electrostatic interaction between Arg5 of TxIA(A10L) and Asp195 in Ac-AChBP and Asp197 in $\alpha_3\beta_2$ nAChRs provides an important energetic contribution to their enhanced affinity at these receptors. In contrast, the activities of TxIA, TxIA(A10L) and PnIA(L5R A10L) at D195A-α_7 were little affected, suggesting that other interactions, probably involving a the hydrophobic patch around position 9/10, dominate α-conotoxin interactions with this subtype.

Comparison between nAChR subtypes

It was an intriguing finding that D195A and D197A mutations had a dramatic effect on TxIA binding at AChBP and $\alpha_3\beta_2$ nAChR, respectively, whereas the corresponding mutation (D195A) in α_7 nAChR barely affected the binding of Arg5-containing conotoxins including TxIA. To help understand this difference, we constructed homology models of both nAChRs and docked TxIA(A10L) into its binding site. Analysis of conotoxin binding in the $\alpha_3\beta_2$ receptor clearly shows that TxIA(A10L) adopts a backbone orientation that is similar to the binding mode observed in our Ac-AChBP co-crystal structure (Figure 5D). This interaction specifically allows an electrostatic interaction between Arg5 and the conserved Asp residue D197, in agreement with our experimental results. To further confirm the existence of this novel binding mode in native $\alpha_3\beta_2$ nAChRs, we utilized a β_2-subunit mutant possessing enhanced hydrophobic contacts between the toxin and receptor (Dutertre *et al*, 2005). As expected, PnIA(L5R A10L) binds to α_3-[V109A]β_2 with an affinity over 10 times higher (0.34 nM, CI 0.30–0.38) than observed at the wild-type receptor (4.6 nM, CI 3.69–5.83) (see Supplementary Figure 4). Interestingly, when this β_2-subunit mutant is coexpressed with the low affinity [D197A]α_3 (2300 nM, CI

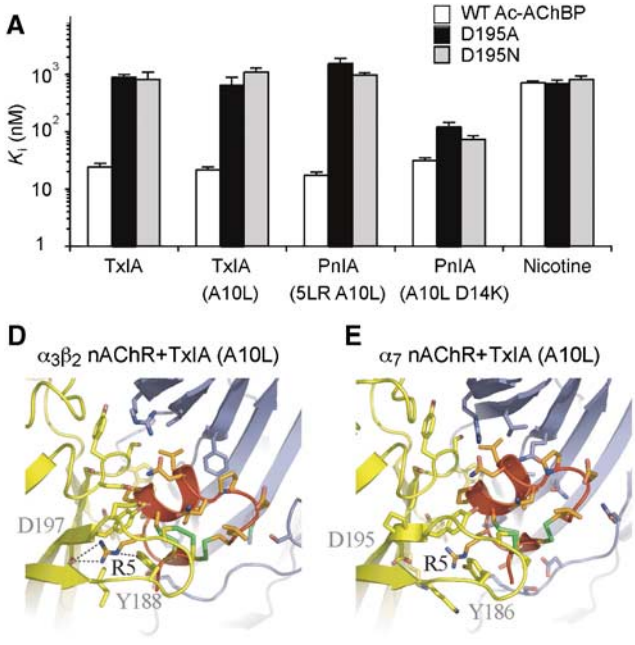

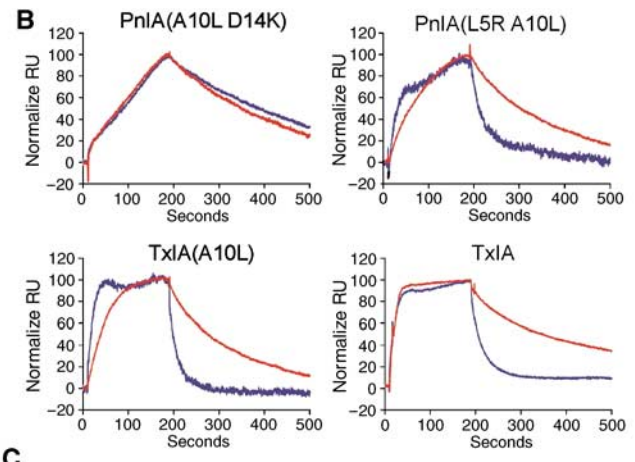

C

	$\alpha_3\beta_2$ nAChR, IC_{50} (CI)		α_7 nAChR, IC_{50} (CI)	
	D197A/WT	D197A	D195A/WT	D195A
TxIA(A10L)	210-fold	421 (354–401)	1.2-fold	46 (34–62)
TxIA	355-fold	1280 (745–2213)	5.3-fold	2100 (1830–2421)
PnIA(L5R A10L)	500-fold	2300 (1780–2966)	2.8-fold	28 (23–34)

Figure 5 Functional contribution of the electrostatic interaction between Arg5-TxIA and an Asp residue of the principal binding subunit of Ac-AChBP and different nAChR subtypes. (**A**) K_i estimates from binding assays on wild-type Ac-AChBP, D195A and D195N mutants demonstrating the loss of affinity for Arg5-containing conotoxins. (**B**) Surface plasmon resonance experiments on wild-type Ac-AChBP (red traces) and D195A mutant (blue traces) for TxIA analogs and PnIA(A10L D14K). (**C**) Effect of the Asp-mutations on the potency of TxIA and analogs to inhibit α_7 and $\alpha_3\beta_2$ nAChR current. (**D, E**) Homology models for the interaction of TxIA(A10L) with $\alpha_3\beta_2$ and α_7 nAChRs. The $\alpha_3\beta_2$ model also shows the Arg–Asp interaction observed in the co-crystal structure.

1780–2966), we observed a dramatic (>100-fold) rescue of PnIA(L5R A10L) affinity (20.5 nM, CI 17.4–24.1). This rescue effect can be explained if the C-terminal hydrophobic half of toxin repositions to interact with $[V109A]\beta_2$, as seen in the Ac-AChBP–PnIA(A10L D14K) co-crystal structure (Celie *et al*, 2005a) compensating for the loss of the energetically favorable Arg5–D197 interaction. Due to conservation in the binding pocket, docking of TxIA(A10L) in the α_7 homology model gave a similar overall result to that obtained using a $\alpha_3\beta_2$ model. However, our experimental results show that, for this subtype, Arg5 is unlikely to interact with D195. TxIA(A10L) was therefore placed in the α_7 binding pocket using the PnIA(A10L D14K) binding mode (Celie *et al*, 2005a) (Figure 5E). This orientation of the conotoxin does not allow a direct interaction between Arg5 and Asp195, explaining the lack of effect the α_7-D195A mutation. Instead, hydrophobic interactions with the complementary side (equivalent of the β-subunit) dominate the binding interaction at α_7.

Finally, mapping the α_7 sequence to the AChBP crystal structure reveals an additional positive charge, Lys184 positioned where it could form an internal salt bridge with Asp195, thus reducing the likelihood of an interaction with Arg5 of TxIA(A10L). In addition, the downward tilt of TxIA(A10L) toward Asp195 might be prevented by a H-bond expected between the TxIA-Leu10 main chain and Gln115 in the α_7 nAChR. Together, these observations support the possibility that TxIA(A10L) binds to α_7 in a conformation observed for ImI and PnIA mutants in the AChBP subtypes. In such a conformation, the relevance of an Arg5-Asp195 salt bridge would be minimized, as has been observed for ImI binding to AChBP. In contrast, the binding to the $\alpha_3\beta_2$ nAChR subtype is likely to be similar to that observed in our AChBP/conotoxin complex, including an important contribution to binding from the Arg5-Asp195 salt bridge.

Discussion

In this study, we demonstrate that an AChBP screen can be used to discover and guide the isolation of new α-conotoxins in crude venom. This rapid and sensitive assay has advantages over fluorescent and electrophysiological methods used previously, and is amenable to high-throughput applications. As all α-conotoxins tested bound to Ls-AChBP in the micromolar to mid nanomolar range, despite having distinct nAChR preferences for muscle and homomeric and heteromeric neuronal nAChR subtypes, it appears that Ls-AChBP has retained ancestral nAChR features that allow a broad range of nAChR ligands to bind. In support, an Ls-AChBP screen of over 30 different cone snail venoms revealed that all significantly displaced ^{125}I-Bgt binding. This high hit-rate supports the hypothesis that each cone snail venom contains at least one nAChR antagonist (McIntosh *et al*, 1999). Given that many cone snails are molluscivorous, and the apparent broad distribution of AChBP in molluscs, AChBP could represent a previously unrecognized molecular target for α-conotoxins with the potential to disrupt molluscan neurotransmission.

The sensitivity of an Ls-AChBP screen is demonstrated with the isolation of α-TxIA, a trace component of *C. textile* venom. The complete pharmacological characterization at Ls-AChBP and nAChRs was subsequently achieved using an identical synthetic form. α-TxIA was found to be the most potent α-conotoxin acting at Ls-AChBP reported to date and also had high affinity for certain mammalian nAChRs. Low nanomolar concentrations of α-TxIA were sufficient to inhibit $\alpha_3\beta_2$ nAChR, whereas 100-fold higher concentrations were needed to block α_7 nAChR current. In contrast, α-OmIA, which also displays high-affinity binding to AChBPs, is equipotent at $\alpha_3\beta_2$ and α_7 nAChRs (Talley *et al*, 2006). Sequence comparison of TxIA with other α-conotoxins and synthesis of selected TxIA analogs revealed important contributions from hydrophobic residues at position 9 and 10 and the key role of Arg5 for high-affinity interactions at Ls-AChBP. Indeed, substitution of Arg5 in PnIA(A10L) produced a gain-of-function analog with similar properties to TxIA. The co-crystal structure of Ac-AChBP in complex with the higher potency analog TxIA(A10L), confirmed the crucial role of Arg5, which is coordinated by Asp195 and Tyr186, an interaction not seen in two other Ac-AChBP–conotoxin complexes (Hansen *et al*, 2005; Celie *et al*, 2005a; Ulens *et al*, 2006). The presence of this salt bridge contributed to a 20° downward tilt of the toxin backbone when compared to PnIA(A10L D14K). An electrostatic interaction was also observed between Arg7 of conotoxin ImI and Asp195 in only one of the two available Ac-AChBP co-crystal structures (PDB accession codes 2BYP and 2C9T). However, mutant cycle analysis has shown that the interaction between Arg7 and Asp197 in nAChRs does not contribute to high-affinity binding of conotoxin ImI (Quiram *et al*, 1999), most likely due to the different orientation of the toxin in the binding site. By mutating Asp195 in the background of Ac-AChBP, we confirmed the functional importance of the electrostatic interaction between Arg5 and Asp195 as observed in the co-crystal structure. Importantly, we observed that the affinity of PnIA(A10L D14K) remains unaffected by Asp195 mutations. This result provides strong evidence that the enhanced affinity of Arg5-containing conotoxins can be attributed to an energetically favorable electrostatic interaction with Asp195 in Ac-AChBP. In combination with electrophysiological recordings on mutant nAChRs, we demonstrated that this conclusion extrapolates to $\alpha_3\beta_2$ nAChRs, but not to α_7 nAChRs. As Asp195 is highly conserved among AChBPs and nAChRs, Arg5 TxIA may share a common set of binding interactions in AChBPs and certain nAChR subtypes.

The reorientation of TxIA(A10L) in the binding pocket of Ac-AChBP is a surprising observation in light of the two other α-conotoxin complexes that we and others have previously determined (Hansen *et al*, 2005; Celie *et al*, 2005a; Ulens *et al*, 2006). Such differences highlight that docking simulations based on the backbone orientation of PnIA(A10L D14K) (Talley *et al*, 2006) or contacts analysis based on superposition of the α-conotoxin backbone (Clark *et al*, 2006) should be interpreted with caution, as these approaches may not adequately address residue changes or the reorientation of side chains in the toxin or receptor, which could generate backbone reorientations as observed for TxIA(A10L). However, from our analysis of homology models, it appears likely that TxIA(A10L) adopts the same orientation in $\alpha_3\beta_2$ nAChRs as seen in our crystal structure, whereas it may adopt a PnIA-like binding orientation in the α_7 nAChR binding pocket. Given this result, it is somewhat surprising that TxIA has no affinity for $\alpha_4\beta_2$ nAChRs despite the presence of an equivalent Asp residue and the close similarity to $\alpha_3\beta_2$

nAChRs across the principal binding face. As no obvious clash could be identified during docking to an $\alpha_4\beta_2$ homology model, it appears that AChBP is not a strong predictor of $\alpha_4\beta_2$ structure, perhaps reflecting different docking pathways or an altered binding site structure.

In conclusion, we have demonstrated that Ls-AChBP can be used to rapidly identify new ligands for nAChRs. By screening the crude venom of different cone snails, we discovered a new α-conotoxin TxIA with enhanced subtype selectivity for $\alpha_3\beta_2$ nAChRs. Co-crystallization of the most potent analog TxIA(A10L) with Ac-AChBP identified a new α-conotoxin binding mode that was stabilized by a critical salt bridge between Arg5-TxIA(A10L) and a highly conserved Asp residue on the principal face of the binding face of Ac-AChBP. The functional importance of this interaction was confirmed through mutagenesis studies in different nAChR subtypes and AChBP. These results establish a structural framework for developing ligands with enhanced selectivity for the $\alpha_3\beta_2$ nAChR. Engineering AChBPs with the ligand-binding sites of specific nAChR subtypes, or with the ligand-binding sites of other ligand-gated ion channels, is expected to identify specific pairwise interactions underlying nAChR selectivity and further expand the potential of this protein scaffold to discover novel pharmacological probes.

Materials and methods

TxIA Isolation, sequencing and mass spectrometry

Venom from *C. textile* specimens was extracted and fractionated as described previously for other cone species (Lewis, 2000). Biological activity was tested using the Ls-AChBP radioligand-binding assay as described previously (Smit *et al*, 2001). This assay directed the final purification of the active compound on analytical RP-HPLC (C_{18} Phenomenex column). A 20 pmol portion of pure peptide was Edman sequenced (Biomolecular Research Facility, Newcastle, Australia) on an Procise HT (Applied Biosystem). Molecular mass analysis of the native and synthetic peptides and LC-MS analysis of crude *C. textile* venom were performed on a C_{18} Phenomenex column (2.1 × 150 mm, 5 μm) eluted with 0 to 60% B in 60 min (A = 0.05% TFA; B = 0.045% TFA, 90% ACN). Eluant was monitored with a PE-Sciex API III triple quadrupole mass spectrometer (Thornhill, Ontario, Canada) over *m/z* 400–2000 and data analyzed using Analyst software (Agilent, CA, USA).

Binding assays

Competitive binding assays with His-tagged Ls-AChBP and ^{125}I-radiolabeled α-bungarotoxin (specific radioactivity 5.5 TBq/mmol) were carried out as described previously (Smit *et al*, 2001). A binding assay was established using P_2 rat brain homogenate as described previously (Rapier *et al*, 1990), with a final protein concentration of 6 mg/ml as determined by a BCA protein assay (Pierce, Rockford, IL, USA). Various concentrations of conotoxins diluted in 200 μl incubation buffer (50 mM HEPES at pH 7.4, 100 mM NaCl, 0.2% BSA) were incubated for 90 min in 100 μl P_2 membrane with a final concentration of 3 nM ^{125}I-α-bungarotoxin to measure binding to α_7 nAChRs, or 1 nM ^{3}H-epibatidine (Amersham Biosciences, Castle Hill, Australia) plus 2 μM cold α-bungarotoxin for non-α_7 nAChRs.

Binding assays with untagged Ac-AChBP and D195 mutants were performed using 5 nM ^{3}H-epibatidine. Ligands were incubated in a white Optiplate-96 (Perkin Elmer) with radioligand and protein (30–120 ng) in binding buffer (PBS, 20 mM Tris at pH 8, 0.05% Tween 20) in a final volume of 100 μl. FlashBlue GPCR beads (2 mg/ml) (Perkin Elmer) were added and after 90 min incubation and 16 h standing in the dark, the radioactivity was measured with a Wallac 1450 MicroBeta liquid scintillation counter. Binding-data were evaluated by a nonlinear, least squares one-site competition curve fitting procedure using Prism 4.01 (GraphPad Software Inc., San Diego, CA, USA).

Protein expression, purification and peptide synthesis

Untagged Ac-AChBP was expressed from baculovirus in SF9 insect cells and purified from medium as described previously (Celie *et al*, 2004). Ac-AChBP D195 mutants were constructed using a QuikChange approach (Stratagene, La Jolla, CA, USA) and verified using DNA sequencing. All peptides were synthesized using Boc chemistry with *in situ* neutralization protocols as described previously (Schnolzer *et al*, 1992). The oxidized peptides were purified by RP-HPLC and analyzed by electrospray mass spectrometry.

Electrophysiology

cDNAs encoding neuronal nAChRs were provided by J. Patrick (Baylor College of Medicine, Houston, TX, USA) and subcloned into the oocyte expression vector pNKS2 (Dutertre *et al*, 2005). Site-directed mutagenesis was performed with the QuikChange mutagenesis Kit (Stratagene, La Jolla, CA, USA) and primers were synthesized by MWG Biotech AG (Ebersberg, Germany). Sequences were verified by didesoxynucleotide sequencing (MWG Biotec AG). cRNA was synthesized from linearized plasmids with SP6 RNA polymerase using the mMessage mMachine kit (Ambion, Austin, TX, USA). *Xenopus laevis* frogs were purchased from Nasco International (Fort Atkinson, WI, USA). Oocytes were prepared as described previously (Dutertre *et al*, 2005) and injected with 50 nl aliquots of cRNA (0.5 μg/μl). Two-electrode voltage-clamp recordings were performed as described previously (Dutertre *et al*, 2005). Current responses to acetylcholine or nicotine were measured 1–10 days after cRNA injection at a holding potential of −70 mV using a Turbo Tec 05X Amplifier (NPI Electronic, Tamm, Germany) and Cell Works software. Currents were filtered at 200 Hz and digitized at 400 Hz. The perfusion medium was automatically switched using a custom-made magnetic valve system. A fast and reproducible solution exchange (<300 ms) was achieved using a 50 μl funnel-shaped oocyte chamber combined with a fast solution flow (~150 μl/s) fed through a custom-made manifold mounted immediately above the oocyte. Agonist pulses were applied for 2 s at 4 min intervals. Peptides were applied for three minutes in a static bath when responses to three consecutive agonist applications differed by less than 10%. EC_{50} values were calculated from a nonlinear fit of the Hill equation to the data (GraphPad version 3.0, San Diego, CA, USA). Data are presented as mean ± s.e. from at least four experiments.

SPR spectroscopy

SPR spectroscopy was performed at 25°C on a Biacore T100 (Uppsala, Sweden). Proteins were immobilized on a CM5 chip using the amine coupling procedure where the proteins at 0.1 mg/ml concentration were flown over the chip at 5 μl/min in 10 mM sodium acetate at pH 4.0. Approximately 5000 response units (RUs) of Ac-AChBP D195A and wild-type Ac-AChBP were immobilized on the chip and the empty flow cell was used as the control. Conotoxins (5–600 nM) in running buffer (25 mM sodium phosphate at pH 8.0, 100 mM sodium chloride) were injected across the chip at 30 μl/min. Biacore T100 evaluation software was used for analysis of the experimental data. GraphPad Prism (GraphPad version 4.0, San Diego, CA, USA) was used to generate final figures.

Crystallography

Crystals of Ac-AChBP in complex with TxIA(A10L) were grown in nanoliter drops by mixing 200 nl protein solution with 200 nl reservoir solution composed of 200 mM sodium malonate, 20% polyethyleneglycol 3350 and bistrispropane at pH 8.5. The crystals belong to spacegroup *P*1 and have the following unit cell dimensions: a = 72.54 Å, b = 85.75 Å, c = 121.67 Å, α = 90.14°, β = 80.01°, γ = 70.64°. Glycerol was used as a cryoprotectant and incrementally added to the mother liquor to a final concentration of 30% before flash-freezing the crystals by immersion in liquid nitrogen. Diffraction data were collected at beamline X06SA at the Swiss Light Source, Villigen. The resolution of observed reflections rapidly decayed from 1.8 to 2.8 Å during a 180° sweep due to radiation sensitivity of the crystals. In addition, the diffraction data showed signs of nonmerohedral twinning. The main crystal lattice was indexed with MOSFLM and data reduction and scaling was carried out with SCALA using the CCP4 program suite (CCP4, 1994). The protein structure was solved by molecular replacement with PHASER (McCoy *et al*, 2005) and the open C-loop structure of Ac-AChBP as the search model (PDB accession code 2C9T). The

initial model was refined to $R_{work} = 27\%$ and $R_{free} = 31\%$ with REFMAC (Murshudov *et al*, 1997) using NCS and TLS restraints (Winn *et al*, 2001). Difference electron density maps clearly indicated the occupancy of all binding sites by TxIA(A10L). The α-conotoxins were built into density with COOT (Emsley and Cowtan, 2004) using the structure of PnIA(A10L D14K) as a template (PDB accession code 2BR8). The model of Ac-AChBP with TxIA(A10L) bound was then further refined to $R_{work} = 24\%$ and $R_{free} = 30\%$. The issue of nonmerohedral twinning was addressed by reprocessing the diffraction data with EVAL14 (Duisenberg *et al*, 2003) and deconvoluting overlapping reflections from the interfering lattice. The resulting electron density map was characterized by a lower noise level, but higher *R*-values for the refined protein model, which is expected due to lack of profile fitting in EVAL14 (Duisenberg *et al*, 2003). Further refinement of the structure was therefore carried out using MOSFLM-processed data. Difference electron density peaks near most of the disulfide bridges in Ac-AChBP and TxIA(A10L) indicated severe radiation damage. Therefore, diffraction data over a 360° sweep were collected on multiple segments of the crystal at beamline EH23-2 of the European Synchrotron Radiation Facility, Grenoble. The beam was attenuated to minimize radiation sensitivity and a merged data set with improved statistics was obtained to 2.4 Å resolution including data to $I/\sigma I = 1$. The model was automatically rebuilt using pyWARP (Cohen *et al*, 2004) and has a $R_{work} = 23\%$ and $R_{free} = 25\%$ with good geometry after iterative cycles of manual rebuilding and refinement. Structure validation was carried out using WHATIF (Hooft *et al*, 1996) and MOLPROBITY (Davis *et al*, 2004). Full molecular replacement and refinement of the data to 2.7 Å, using a more conservative data cut-off ($I/\sigma I = 2$), showed that the electron density did not change, but automatic rebuilding failed, indicating that the weak data contained significant information and that any errors in their measurement were sufficiently reduced by the use of maximum likelyhood refinement. Coordinates have been deposited in the Protein Data Bank with accession code 2UZ6. AREAIMOL and CONTACT were used to analyze interaction surface areas and contacts (CCP4, 1994). Interaction surface areas are reported as average ± s.d. of binding sites occupied by conotoxin and in the context of the number of pentamers present in the asymmetric unit. Interactions between residues of conotoxins and Ac-AChBP were only considered if present in at least three of five binding sites. Figures were prepared with PYMOL (DeLano Scientific, San Carlos, CA, USA).

Molecular modeling

The crystal structure of TxIA(A10L) bound to Ac-AChBP was used as a template to build homology models of rat α_7, $\alpha_3\beta_2$ and $\alpha_4\beta_2$ nAChRs following the method described by Dutertre *et al* (2005).

Supplementary data

Supplementary data are available at *The EMBO Journal* Online (http://www.embojournal.org).

Acknowledgements

We thank Marion Loughnan for the gift of α-conotoxins EI and [Y15]-EpI, Alun Jones for mass spectrometry assistance, Laurent Billot for his help with statistical analysis, beamline staff at ESRF and SLS for assistance with data collection, Tassos Perrakis for advise on data collection and processing, members of the Sixma and Perrakis laboratory for comments and suggestions. Toine Schreurs and Loes Kroon-Batenburg are acknowledged for processing data with EVAL, Serge Cohen for test driving pyWARP, Judith Smit for assisting with AChBP cloning and protein purification, Victor Tsetlin for donating PnIA(A10L D14K) and Heinrich Betz for generous support. This work was supported by an NHMRC Program Grant and Australian Research Council grant (RJL and PFA), a postgraduate scholarship from the University of Queensland (SD), the Deutsche Forschungsgemeinschaft NI 592/3 (AN) and a long-term fellowship from the European Molecular Biology Organization (CU) as well as STW grant BBC6035 to TKS and ABS.

References

Bourne Y, Talley TT, Hansen SB, Taylor P, Marchot P (2005) Crystal structure of a Cbtx-AChBP complex reveals essential interactions between snake α-neurotoxins and nicotinic receptors. *EMBO J* **24:** 1512–1522

CCP4 (1994) The CCP4 suite: programs for protein crystallography. *Acta Crystallogr D* **50:** 760–763

Celie PH, Kasheverov IE, Mordvintsev DY, Hogg RC, van Nierop P, van Elk R, van Rossum-Fikkert SE, Zhmak MN, Bertrand D, Tsetlin V, Sixma TK, Smit AB (2005a) Crystal structure of nicotinic acetylcholine receptor homolog AChBP in complex with an α-conotoxin PnIA variant. *Nat Struct Mol Biol* **12:** 582–588

Celie PH, Klaassen RV, van Rossum-Fikkert SE, van Elk R, van Nierop P, Smit AB, Sixma TK (2005b) Crystal structure of acetylcholine-binding protein from *Bulinus truncatus* reveals the conserved structural scaffold and sites of variation in nicotinic acetylcholine receptors. *J Biol Chem* **280:** 26457–26466

Celie PH, van Rossum-Fikkert SE, van Dijk WJ, Brejc K, Smit AB, Sixma TK (2004) Nicotine and carbamylcholine binding to nicotinic acetylcholine receptors as studied in AChBP crystal structures. *Neuron* **41:** 907–914

Clark RJ, Fischer H, Nevin ST, Adams DJ, Craik DJ (2006) The synthesis, structural characterization, and receptor specificity of the α-conotoxin Vc1.1. *J Biol Chem* **281:** 23254–23263

Cohen SX, Morris RJ, Fernandez FJ, Ben Jelloul M, Kakaris M, Parthasarathy V, Lamzin VS, Kleywegt GJ, Perrakis A (2004) Towards complete validated models in the next generation of ARP/wARP. *Acta Crystallogr D* **60:** 2222–2229

Davis IW, Murray LW, Richardson JS, Richardson DC (2004) MOLPROBITY: structure validation and all-atom contact analysis for nucleic acids and their complexes. *Nucleic Acids Res* **32:** W615–W619

Dutertre S, Nicke A, Lewis RJ (2005) β2 subunit contribution to 4/7 α-conotoxin binding to the nicotinic acetylcholine receptor. *J Biol Chem* **280:** 30460–30468

Duisenberg AJM, Kroon-Batenburg LMJ, Schreurs AMM (2003) An intensity evaluation method: EVAL-14. *J Appl Cryst* **36:** 220–229

Emsley P, Cowtan K (2004) Coot: model-building tools for molecular graphics. *Acta Crystallogr D* **60:** 2126–2132

Everhart D, Cartier GE, Malhotra A, Gomes AV, McIntosh JM, Luetje CW (2004) Determinants of potency on α-conotoxin MII, a peptide antagonist of neuronal nicotinic receptors. *Biochemistry* **43:** 2732–2737

Hansen SB, Sulzenbacher G, Huxford T, Marchot P, Taylor P, Bourne Y (2005) Structures of *Aplysia* AChBP complexes with nicotinic agonists and antagonists reveal distinctive binding interfaces and conformations. *EMBO J* **24:** 3635–3646

Hansen SB, Talley TT, Radic Z, Taylor P (2004) Structural and ligand recognition characteristics of an acetylcholine-binding protein from *Aplysia californica*. *J Biol Chem* **279:** 24197–24202

Hogg RC, Miranda LP, Craik DJ, Lewis RJ, Alewood PF, Adams DJ (1999) Single amino acid substitutions in α-conotoxin PnIA shift selectivity for subtypes of the mammalian neuronal nicotinic acetylcholine receptor. *J Biol Chem* **274:** 36559–36564

Hooft RW, Vriend G, Sander C, Abola EE (1996) Errors in protein structures. *Nature* **381:** 272

Lewis RJ (2000) Ion channel toxins and therapeutics: from cone snail venoms to ciguatera. *Ther Drug Monit* **22:** 61–64

Lewis RJ, Garcia ML (2003) Therapeutic potential of venom peptides. *Nat Rev Drug Discov* **2:** 790–802

Loughnan ML, Alewood PF (2004) Physico-chemical characterization and synthesis of neuronally active α-conotoxins. *Eur J Biochem* **271:** 2294–2304

Luo S, Nguyen TA, Cartier GE, Olivera BM, Yoshikami D, McIntosh JM (1999) Single-residue alteration in α-conotoxin PnIA switches its nAChR subtype selectivity. *Biochemistry* **38:** 14542–14548

McCoy AJ, Grosse-Kunstleve RW, Storoni LC, Read RJ (2005) Likelihood-enhanced fast translation functions. *Acta Crystallogr D* **61:** 458–464

McIntosh JM, Santos AD, Olivera BM (1999) *Conus* peptides targeted to specific nicotinic acetylcholine receptor subtypes. *Annu Rev Biochem* **68:** 59–88

Murshudov GN, Vagin AA, Dodson EJ (1997) Refinement of macromolecular structures by the maximum-likelihood method. *Acta Crystallogr D* **53:** 240–255

Olivera BM, Rivier J, Clark C, Ramilo CA, Corpuz GP, Abogadie FC, Mena EE, Woodward SR, Hillyard DR, Cruz LJ (1990) Diversity of *Conus* neuropeptides. *Science* **249:** 257–263

Quiram PA, Jones JJ, Sine SM (1999) Pairwise interactions between neuronal α7 acetylcholine receptors and α-conotoxin ImI. *J Biol Chem* **281:** 19517–19524

Rapier C, Lunt GG, Wonnacott S (1990) Nicotinic modulation of [^{3}H]dopamine release from striatal synaptosomes: pharmacological characterisation. *J Neurochem* **54:** 937–945

Satkunanathan N, Livett B, Gayler K, Sandall D, Down J, Khalil Z (2005) α-Conotoxin Vc1.1 alleviates neuropathic pain and accelerates functional recovery of injured neurones. *Brain Res* **1059:** 149–158

Schnolzer M, Alewood P, Jones A, Alewood D, Kent SB (1992) *In situ* neutralization in Boc-chemistry solid phase peptide synthesis. Rapid, high yield assembly of difficult sequences. *Int J Pept Protein Res* **40:** 180–193

Smit AB, Syed NI, Schaap D, van Minnen J, Klumperman J, Kits KS, Lodder H, van der Schors RC, van Elk R, Sorgedrager B, Brejc K, Sixma TK, Geraerts WP (2001) A glia-derived acetylcholine-binding protein that modulates synaptic transmission. *Nature* **411:** 261–268

Talley TT, Olivera BM, Han KH, Christensen SB, Dowell C, Tsigelny I, Ho KY, Taylor P, McIntosh JM (2006) α-Conotoxin OmIA is a potent ligand for the acetylcholine-binding protein as well as α3β2 and α7 nicotinic acetylcholine receptors. *J Biol Chem* **281:** 24678–24686

Ulens C, Hogg RC, Celie PH, Bertrand D, Tsetlin V, Smit AB, Sixma TK (2006) Structural determinants of selective α-conotoxin binding to a nicotinic acetylcholine receptor homolog AChBP. *Proc Natl Acad Sci USA* **103:** 3615–3620

Vincler M, Wittenauer S, Parker R, Ellison M, Olivera BM, McIntosh JM (2006) Molecular mechanism for analgesia involving specific antagonism of α9α10 nicotinic acetylcholine receptors. *Proc Natl Acad Sci USA* **103:** 17880–17884

Winn MD, Isupov MN, Murshudov GN (2001) Use of TLS parameters to model anisotropic displacements in macromolecular refinement. *Acta Crystallogr D* **57:** 122–133